J Mater Sci (2010) 45:5077–5083
DOI 10.1007/s10853-010-4353-3

ICAM 2009

First-order-reversal-curve analysis of Pr–Fe–B-based exchange spring magnets

D. R. Cornejo · T. R. F. Peixoto · S. Reboh · P. F. P. Fichtner · V. C. de Franco · V. Villas-Boas · F. P. Missell

Received: 30 November 2009 / Accepted: 24 February 2010 / Published online: 9 March 2010
© Springer Science+Business Media, LLC 2010

Abstract Ribbons of nominal composition $(Pr_{9.5}Fe_{84.5}B_6)_{0.96}Cr_{0.01}(TiC)_{0.03}$ were produced by arc-melting and melt-spinning the alloys on a Cu wheel. X-ray diffraction (XRD) reveals two main phases, one based upon α-Fe and the other upon $Pr_2Fe_{14}B$. The ribbons show exchange spring behavior with $H_c = 12.5$ kOe and $(BH)_{max} = 13.6$ MGOe when these two phases are well coupled. Transmission electron microscopy revealed the coupled behavior is observed when the microstructure consists predominantly of α-Fe grains (diameter ~100 nm.) surrounded by hard material containing $Pr_2Fe_{14}B$. The microstructure is discussed in terms of a calculation by Skomski and Coey. A first-order-reversal-curve (FORC) analysis was performed for both a well-coupled sample and a poorly coupled sample. The FORC diagrams show two strong peaks for both the poorly coupled sample and for the well-coupled material. In both cases, the localization of the FORC probability suggests magnetizing interactions between particles. Switching field distributions were calculated and are consistent with the sample microstructure.

D. R. Cornejo · T. R. F. Peixoto
Instituto de Física, Universidade de São Paulo, C. P. 66318, Sao Paulo, SP 05508-900, Brazil

S. Reboh
Groupe nMat, CEMES-CNRS, 29 rue J. Marvig, 31055 Toulouse, France

P. F. P. Fichtner
Engineering School, Federal University of Rio Grande do Sul, Porto Alegre, Brazil

V. C. de Franco · V. Villas-Boas · F. P. Missell (✉)
Centro de Ciências Exatas e Tecnologia, Universidade de Caxias do Sul, Caxias do Sul, RS 95070-560, Brazil
e-mail: fmissell@yahoo.com

Introduction

Remanence enhancement was first observed experimentally by two groups [1, 2], while the general principle behind exchange spring magnets was later proposed by Kneller and Hawig [3]: nanometer-sized grains of a hard magnetic material may couple to grains of a magnetically soft material to produce both remanence enhancement and a highly reversible second quadrant susceptibility. More recent reviews of magnetic nanostructures [4, 5] have considered the length scales encountered in exchange spring magnets and their effect on magnetic properties and specifically on magnetization reversal and coercivity.

Although remanence enhancement was noticed early on, low values of the coercive field H_c prevented widespread use of these materials. However, several groups investigated the use of additives to enhance H_c. The effect of a wide range of transition metal carbides on the glass forming ability of $Nd_2Fe_{14}B$ alloys was investigated [6, 7]. Branagan and McCallum [8] found that Ti addition to Nd–Fe–B alloys leads to the suppression of α-Fe dendrites. The addition of TiC to $Nd_2Fe_{14}B$ + α-Fe nanocomposites resulted in improved control of the microstructure over a larger fraction of the ribbon volume and an improvement in the magnetic properties [9]. Chang et al. [10] demonstrated that Ti suppresses the formation of the metastable cubic $Pr_2Fe_{23}B_3$ phase in Pr–Fe–B alloys. The addition of C to the composition prevents the formation of detrimental TiB_2 and also favors grain refinement.

Another approach to increasing coercivity was taken by Hirosawa and coworkers [11, 12] who added small amounts of Cr to Nd-poor alloys to enhance H_c. In Ref. [12] the crystallization kinetics of amorphous melt-spun ribbons was studied using X-ray diffraction and Mossbauer spectroscopy. Hyperfine fields of the Fe_3B and Fe_2B phases

were found to be reduced by the addition of Cr in agreement with other Mossbauer results [13]. The kinetics of the reactions whereby the Cr increases the amount of the hard magnetic phase present in the material were elucidated. Similar increases in the coercivity of PrFeB alloys with Cr additions have been observed [14, 15]. Recent studies of rare-earth-rich Nd–Fe–B [16] and Pr–Fe–B-based [17, 18] materials doped with both Ti–C and Cr have shown that it is possible to obtain H_c up to 20 kOe, sufficient for many applications.

This article deals with microstructure and magnetic interactions in rare-earth-rich Pr–Fe–B-based spring magnets (containing Ti, C, and Cr), where the hard magnetic phase is $Pr_2Fe_{14}B$ and the soft magnetic phase is α-Fe. Recent studies [19, 20] have shown that Ti–C additions to rare-earth-rich Pr–Fe–B-based materials have a very beneficial effect on coercivity. That increase in H_c is more pronounced when small amounts of Cr are included [17]. Mossbauer spectroscopy had previously been used to show [17] that the Cr modified the hyperfine fields of the $Nd_2Fe_{14}B$ phase, while the α-Fe was left unchanged. This is in contrast to the rare-earth-poor materials [12, 13] where the hard magnetic phase does not seem to be modified by Cr substitutions, although the hyperfine fields of the Fe_3B and Fe_2B phases were found to be reduced. The alloy studied here presents a very interesting microstructure. Indeed, transmission electron microscopy showed that our samples present an unusual structure consisting of roughly spherical grains of α-Fe (with diameters around ~100 nm) immersed in a matrix of $Pr_2Fe_{14}B$. In spite of their large size, the grains of the soft phase are well coupled to the hard phase (sample WCS), as demonstrated by the hysteresis loop of the as-cast material. Moderate heat treatments (for example, 5–10 min at 680 °C) are sufficient for the grains to grow and for the phases to decouple (sample UCS).

We discuss the coupling between the two phases in terms of the nucleation field for magnetization reversal of α-Fe in this geometry [21]. The magnetic interactions in this system were studied using a formalism employing first-order-reversal-curves (FORCs) [18]. The FORC distribution provides a detailed characterization of the hysteretic response of a magnetic system [22–24] to an applied field by revealing the dominant interactions in the system, the magnetic viscosity effects, and the destruction of memory during a demagnetization process.

Experiment

Alloys of composition $(Pr_{9.5}Fe_{84.5}B_6)_{0.96}Cr_{0.01}(TiC)_{0.03}$ were produced by melting the elements in an arc furnace. (Both samples studied here (WCS and UCS) have this composition.) Ribbons with thickness in the range 40–60 μm were obtained by melt-spinning the alloys on a rapidly rotating Cu wheel in a He atmosphere. A wheel speed of roughly 20 m/s was found to produce a nanocrystalline composite with optimal magnetic properties. Previously [17] we showed that annealing the as-cast materials, even for very short times (3 min), led to a reduction in the coercive field. As mentioned previously, a moderate heat treatment of sample WCS for 5–10 min at 680 °C is sufficient for the grains to grow and for the phases to decouple (sample UCS).

X-ray diffraction data of the nanocrystalline composites were collected with a PW1710 diffractometer ($\lambda =$ 1.5405 Å). Previously, a Rietveld analysis [in Ref. 17] of a sample without Cr showed essentially two phases, $Pr_2Fe_{14}B$ (68 wt%) with lattice parameters $a = 0.881$ nm and $c = 1.222$ nm, and α-Fe (32 wt%) with $a = 0.288$ nm. In the XRD patterns of samples with Cr, no substantial differences in the peaks positions and relative intensities were detected. Transmission electron microscopy (TEM) and (qualitative) energy-dispersive X-ray analysis (EDS) were carried out in a JEOL JEM-2010 microscope operating at 200 kV. The plan-view specimens were prepared by mechanical grinding.

The magnetic properties were measured with a vibrating sample magnetometer mounted on a 90 kOe superconducting magnet. For the as-cast alloy [with composition $(Pr_{9.5}Fe_{84.5}B_6)_{0.96}Cr_{0.01}(TiC)_{0.03}$] the coercivity and the maximum energy product were $H_c = 12.5$ kOe and $(BH)_{max} = 13.6$ MGOe, respectively [17]. In Fig. 1 of Refs. [17, 18], a hysteresis curve for this composition [$(Pr_{9.5}Fe_{84.5}B_6)_{0.96}Cr_{0.01}(TiC)_{0.03}$] (denoted Pr–1% Cr) was compared to one for a sample without [$Cr(Pr_{9.5}Fe_{84.5}B_6)_{0.97}(TiC)_{0.03}$] (denoted Pr–0% Cr) to illustrate the effect of Cr on H_c. In general, the as-cast ribbons showed good coupling between hard and soft phases, as shown previously [17, 18].

A set of FORCs was obtained by: (i) saturating the sample by applying a field H_{max}, (ii) reducing the field to a return value H_r where $H_r < H_{max}$, (iii) increasing H to H_{max} again and measuring the magnetization, and (iv) repeating steps (ii) and (iii) for decreasing values of H_r where $H_r > -H_{max}$. Figure 1 shows the FORCs thus obtained for WCS and UCS. For each sample, one of the FORCs has been highlighted for later discussion. The FORC distribution ρ may then be defined in terms of the magnetization $M(H_r,H)$ by the mixed derivative

$$\rho(H_r, H) = -\frac{1}{2}\frac{\partial^2 M(H_r, H)}{\partial H_r \partial H}$$

which is plotted in a rotated system of coordinates $\{H_c,H_b\}$ given by $\{H_c = ½(H - H_r),\ H_b = ½(H + H_r)\}$. In this coordinate system, ρ can be compared with a statistical

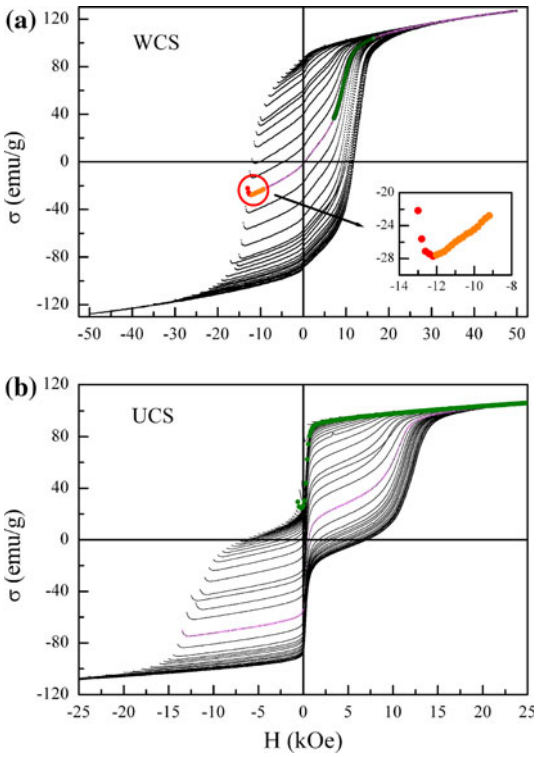

Fig. 1 First-order-reversal-curves (FORCs) obtained at room temperature for **a** the well-coupled sample and **b** a poorly coupled sample. Several individual FORCs have been highlighted to facilitate discussion below. The *inset* shows the effect of magnetic viscosity on the FORC

distribution of particles characterized by coercive and bias fields H_c and H_b, respectively. For each sample, a set of approximately 90 FORCs was measured using a field sweep rate of around 70 Oe/s, i.e., a value sufficiently low to reduce the presence of dynamic effects in the FORC diagrams [18, 25]. Also, in order to avoid errors in the interpretations of the FORC diagrams a magnetic field step of 10 Oe (much smaller than the coercivity of the soft phase) was used.

Results and discussion

Microstructure

The TEM analysis of the WCS sample shows a principal characteristic microstructure. This dominant microstructure is shown in Fig. 2, where the qualitative EDS analysis indicates that the light colored grains contain only Fe, while Pr is concentrated in the darker surrounding regions. The diameter D of the light grains in the well-coupled sample was estimated to be about 100 nm (see inset in Fig. 2). This value is in excellent agreement with diameters reported previously [17] on another sample with 1% Cr, measured at a different laboratory. As a further check on

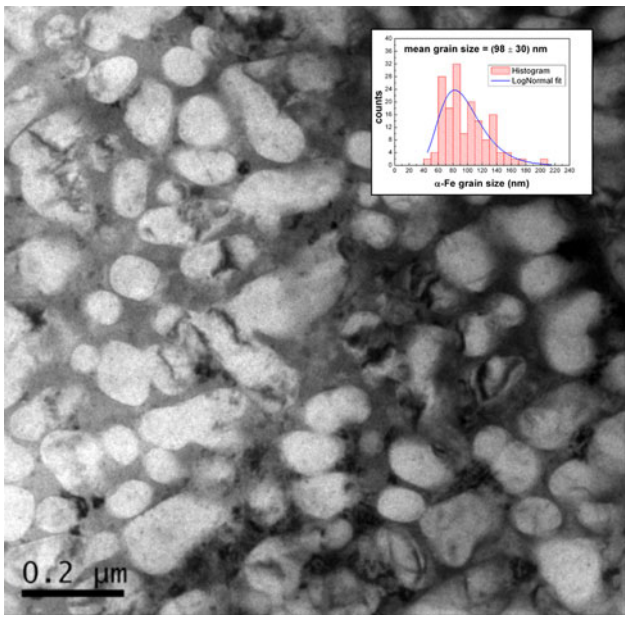

Fig. 2 Dominant microstructure in a well-coupled sample (sample WCS). Light grains contain only Fe. The *inset* shows the distribution of (*light*) grain diameters

the microstructure, we considered a simple model in which 100 nm diameter spheres of α-Fe were placed inside cubes of side a containing $Pr_2Fe_{14}B$ outside of the sphere. Using the proportions of the two phases from the Rietveld analysis mentioned above, the cube edge is found to be $a \sim 120$ nm, a reasonable result. This shows that the microstructure of Fig. 2 is consistent with the Rietveld analysis of the X-ray diffraction data.

It is interesting, furthermore, to consider the microstructure of Fig. 2 in relation to those shown in Ref. [26] for Nd-poor and B-rich Nd–Fe–B materials containing Ti and C. In that case [26], the microstructure was found to consist of much smaller hard magnetic grains surrounded by a soft, Fe-rich intergranular phase. Those authors considered a microstructure consisting of primary Fe surrounded by a hard magnetic phase to be unfavorable for achieving good coercivity values. Our results show that soft grains surrounded by hard material also provides a satisfactory microstructure for high-coercivity nanocomposite magnets.

The exchange length for Pr–Fe–B can be estimated to be about 2 nm, although Skomski [4] suggests that, in practice, this value might be increased by a factor 5. Although our results seem to show that it may not be necessary to have an exact match between grain size and exchange length to have high coercivity, one must consider the relation between the two fundamental length scales of this problem. If we suppose the exchange length to have its most favorable value ($l_{ex} \sim 10$ nm), this still leaves us with a grain of effective diameter $D_{eff} = D - 2l_{ex} = 80$ nm with low anisotropy. See Fig. 3.

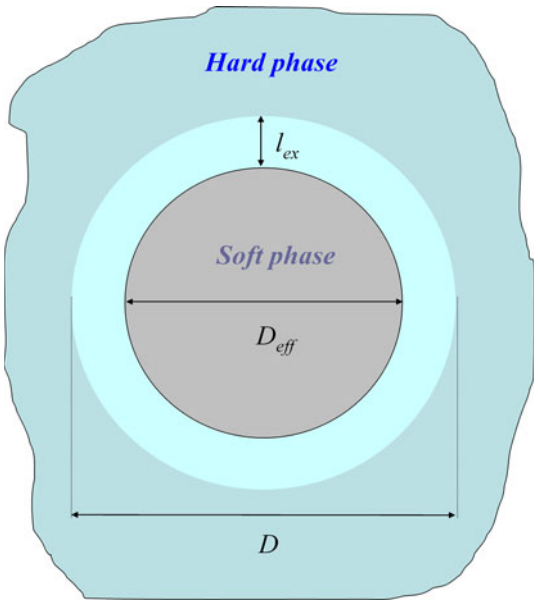

Fig. 3 Schematic representation of a grain of α-Fe surrounded by hard magnetic $Pr_2Fe_{14}B$. A region with effective diameter $D_{eff} = D - 2l_{ex}$ has low anisotropy

The problem of a soft grain surrounded by ordered hard magnetic material was considered by Skomski and Coey [21, 27] some years ago using a micromagnetic approach. These authors found that the nucleation field of a soft sphere in a hard matrix is given by the solution of the following eigenvalue equation:

$$\frac{A_s}{A_h}\left[\frac{D}{2}\sqrt{\mu_0 M_s H_n/2A_s}\cot\left(\frac{D}{2}\sqrt{\mu_0 M_s H_n/2A_s}\right) - 1\right] + 1 + \frac{D}{2}\sqrt{(2K_h - \mu_0 M_h H_n)/2A_h} = 0$$

In this equation, A_h (A_s), M_h (M_s), and K_h are the exchange constant, the saturation magnetization, and the anisotropy constant of the hard (soft) phase. We solved this equation numerically and calculated the value of the nucleation field as a function of the particle diameter using the following values: $\mu_0 M_h = 1.56$ T, $\mu_0 M_s = 2.15$ T, $A_s = 1.67 \times 10^{-11}$ J/m, $A_h = 1.07 \times 10^{-11}$ J/m, $K_h = 6 \times 10^6$ J/m^3. The result of this calculation is shown in Fig. 4. Considering the distribution of particle diameters shown in the histogram of Fig. 2, we estimate that about 2/3 of the Fe particles (those with effective diameters below 90 nm) would have nucleation fields above 3.5 kOe, which is considerably higher than the nucleation field of pure Fe. The peak of the histogram corresponds to a nucleation field of about 6 kOe. The magnetic hardness of this system would be destroyed by the coalescence of the soft particles or if their separation were less than a domain wall width of the hard material (~4 nm.), which appears not to be the case. Figure 4 also shows that the grain size increase produced by annealing (sample UCS) is sufficient to reduce

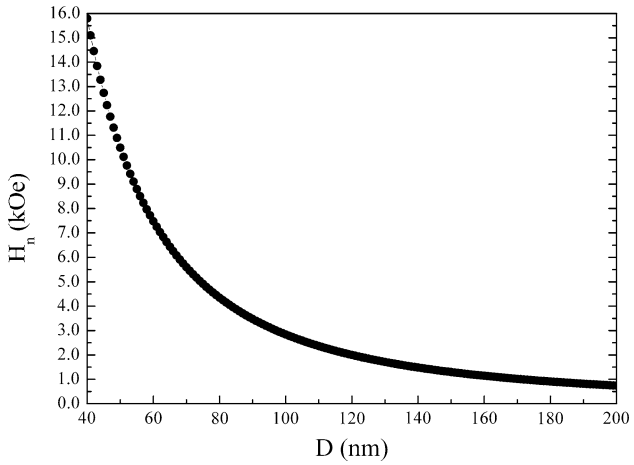

Fig. 4 The nucleation field of a soft particle in a hard matrix versus particle size, calculated using the theory from Refs. [21, 27] with values $\mu_0 M_h = 1.56$ T, $\mu_0 M_s = 2.15$ T, $A_s = 1.67 \times 10^{-11}$ J/m, $A_h = 1.07 \times 10^{-11}$ J/m, $K_h = 6 \times 10^6$ J/m^3

the nucleation fields of the α-Fe grains, which may lead to an uncoupling of the hard and soft phases.

Magnetic interactions

The FORC distributions $\rho(H_b, H_c)$ generated in our analysis are shown in Figs. 5 and 6 for the two samples considered. Both distributions show peaks associated with two different regions that we have denominated as the "hard" contribution and the "soft" contribution. The peak positions are given in Table 1.

In both Figs. 5 and 6, it is possible to see a ridge near $H_c = 0$, associated with the rotation of low-coercivity particles (particles with H_c up to ~1.5 kOe in Figs. 5 and 6). This is the soft contribution, and it is predominantly located at $H_b < 0$. It is possible to see, following the highlighted FORCs in Fig. 1 and the corresponding lines in Figs. 5 and 6, this contribution is produced by the remagnetization of those particles that initially reverted (because of the magnetic viscosity) when the magnetic field is returned to H_{max}. As was mentioned in "Experiment" section, a field sweep rate of 70 Oe/s was used in the measuring process. This value was sufficient to reduce the dynamic effects in the FORC diagrams, but still did not eliminate them, as can be deduced from the initial decrease of the magnetization in the FORCs (see the inset of Fig. 1a). This region of the FORC, circled in Fig. 1a, is effectively responsible for the ridge in the respective FORC diagram, as can be deduced by observing the circle in Fig. 5 (together with that of Fig. 1a). Studies in films of $Pd_{80}Co_{20}$ [25] and simulations using the dynamic Preisach model [28] showed that the intensity of those ridges is strongly dependent on the field sweep rate. However, its position seems not to be affected by this variable.

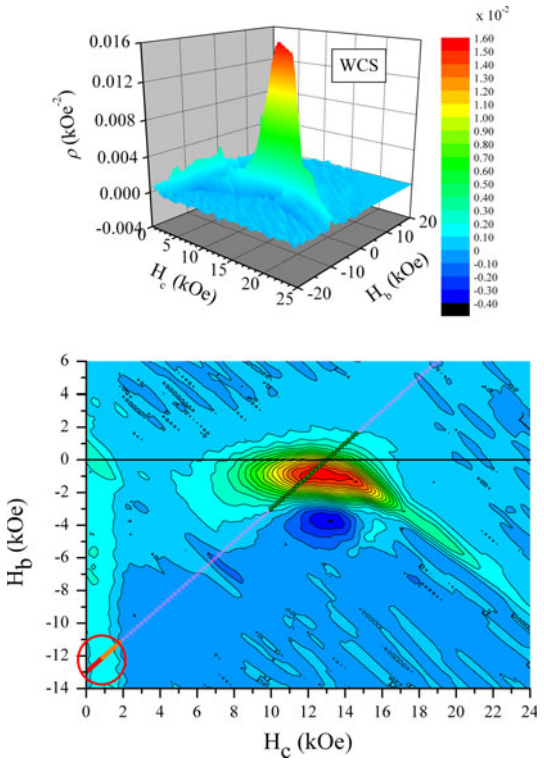

Fig. 5 The FORC distribution $\rho(H_b, H_c)$ for the well-coupled sample. The colored diagonal line in the lower part of the figure was derived from the highlighted FORC of Fig. 1a and its two nearest neighbors. The circle shown in the "ridge" region corresponds to the *inset* of Fig. 1a

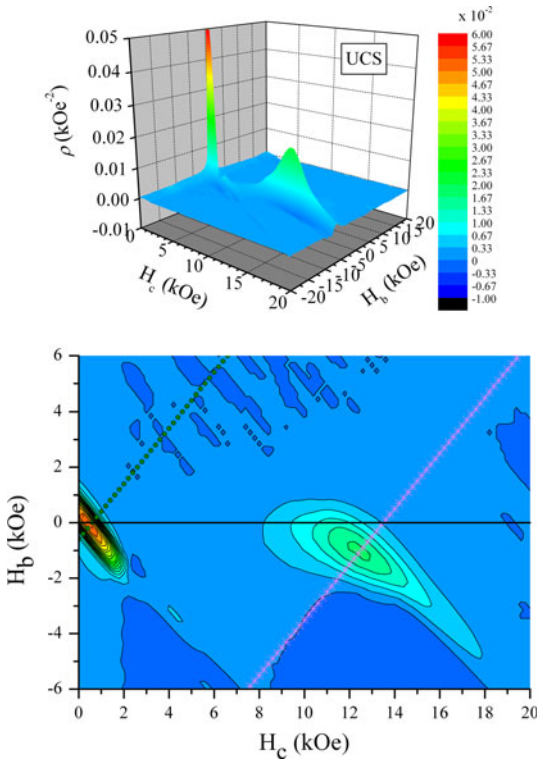

Fig. 6 The FORC distribution $\rho(H_b, H_c)$ for the poorly coupled sample. The colored diagonal lines in the lower part of the figure were derived from the highlighted FORCs of Fig. 1 and their two nearest neighbors

The amplitude of the soft contribution in WCS is not as great as in UCS, although the peak positions are approximately the same in the two samples. However, their relative weights are very different. (Note that the probability associated with a peak in $\rho(H_b, H_c)$ is not given by the height of the peak, but rather by the integral of the area under the peak.) One can imagine that the soft contribution arises principally in those grains of α-Fe that are not totally exchange-coupled to the $Pr_2Fe_{14}B$ phase. The histogram shown as an inset in Fig. 2 displays the grain size distribution which can be approximated by a log-normal function. A certain fraction of this distribution corresponds to large grains. As we have seen above, when these large grains are surrounded by $Pr_2Fe_{14}B$, they may present high coercivity values. An increase in grain size due to annealing would give rise to more grains of greater size, with lower coercivity values.

From Figs. 1, 5, and 6, one can surmise that the hard contribution to the magnetization is associated with magnetization reorientation in particles with coercivities in the range 7–17 kOe (WCS) or 5–12 kOe (UCS). Following our reasoning, the hard contribution in the FORC distributions must correspond to the $Pr_2Fe_{14}B$ phase as well as the Fe atoms which are tightly coupled to the hard phase, i.e., Fe atoms in the shell of thickness l_{ex} in Fig. 3 as well as those

Table 1 Peak positions of the FORC distributions for the two samples

Sample	Region	H_b (Oe)	H_c (Oe)
UCS	Soft	−150	560
	Hard	−950	12300
WCS	Soft	−150	560
	Hard	−750	12400

in grains with *effective diameters* smaller than about 60 nm for WCS and about 75 nm for UCS (see Fig. 4). The hard contribution is clearly predominant in sample WCS, and the peak in ρ appears at slightly higher magnetic field values than in UCS. In Ref. [24] Pike and coauthors, studying a strongly ordered perpendicular nickel nanopillar array, associated a curved FORC distribution with the peak shifted along H_b and exhibiting a negative region (three features that are exhibited by the FORC diagrams of our samples WCS and UCS), to the presence of a mean interaction field of the form $H_{int} = -JM$. In the analysis and simulations presented by those authors a positive (negative) interaction parameter J produces a shift of the distribution to the positive (negative) H_b region. Then, it is possible to associate the negative H_b displacements exhibited by our diagrams to magnetizing interactions

between magnetic grains of the samples. This behavior is expected in a well-coupled exchange spring magnet where the remanence enhancement is clearly observed ($M_r/M_S \approx 0.60$ for the WCS). However, it is not clear why this behavior is also present in the uncoupled sample, where the hard peak is shifted to more negative values of H_b. The heterogeneous nature of the UCS sample (as opposed to the more "uniform" behavior of WCS) suggests that the mechanism which led to the negative H_b displacement, may, in this case, be quantitatively different from that in the WCS sample: in effect, the reversal of the hard grains occurs in an environment where the soft phase has already been reversed. It is interesting to note that the shift of the hard peak to negative H_b values was also observed in the experimental FORC distributions presented by Chiriac et al. [29] for NdDyFeCoB nanocomposites.

Using the experimental FORC distributions, we may calculate the switching field distributions SFD for each sample. SFD is given in terms of the integral [30]

$$\mathrm{SFD} = \frac{\mathrm{d}M(H_r)}{\mathrm{d}H_r} = \int \rho(H, H_r)\mathrm{d}H$$

The results are shown in Fig. 7 below. Both experimental curves can be seen to show two peaks. The experimental SFD curves were fitted to a pair of Lorentzians, and this result is also shown in Fig. 7. It is interesting to compare the area associated with the two Lorentzians for the two samples. In the case of the well-coupled sample (WCS), 81% of the area is associated with the hard phase and 19% with the soft phase. For sample UCS, 54% of the area is associated with the hard phase and 46% with the soft phase. These results suggest that a certain (high) fraction of the hard phase must be present in order to observe the well-coupled behavior.

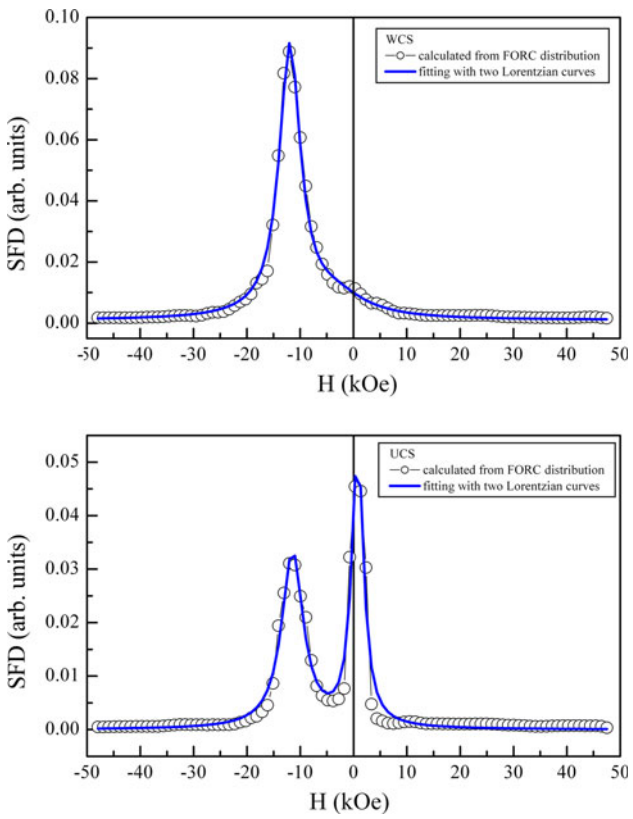

Fig. 7 Switching field distributions SFD for the two samples

Finally, Chiriac et al. [29] applied the FORC formalism to study bulk rare-earth-poor Nd–Fe–B-based nanocomposites where the hard phase was $Nd_2Fe_{14}B$ and the soft phases were Fe_3B and α-Fe. It is interesting to consider the micromagnetic calculations used by Chiriac et al. [29, 31] to simulate the magnetization behavior of several samples and their FORC diagrams. Simulated FORC diagrams for different ratios of hard and soft phases showed significant changes in the coupling of magnetic phases when the percentage of hard phase was reduced from 85 to 65%. This behavior appears to be similar to that which we have observed in the Pr–Fe–B nanocomposites.

Conclusions

This study has shown that the high coercive fields, first observed for Nd–Fe–B spring magnets with small additions of Ti, C, and Cr by Ishii et al. [16], can also seen in Pr–Fe–B spring magnets with similar doping. Furthermore, TEM observations have shown a rather unusual microstructure where large (~100 nm) grains of α-Fe are surrounded by a hard Pr–Fe-based phase. This microstructure seems to be consistent with the micromagnetic calculations of Skomski and Coey [21, 27] who treated the nucleation field of a soft sphere in a hard matrix.

A first-order-reversal-curve analysis was performed on two samples, one of which showed good coupling between the phases and the other showing poor coupling. Both hard and soft contributions were readily identified. The soft contribution arises principally in those grains of α-Fe that are not totally exchange-coupled to the $Pr_2Fe_{14}B$ phase. Experimental switching field distributions were calculated from the FORC distributions which are consistent with different proportions of hard and soft phases in the two samples.

Acknowledgements This study was supported by the Brazilian agencies Conselho Nacional de Desenvolvimento Científico e Tecnológico (CNPq), Fundação de Amparo à Pesquisa do Estado de São Paulo (FAPESP), and Financiadora de Estudos e Projetos (FINEP).

References

1. McCallum RW, Kadin AM, Clemente GB, Keem JE (1987) J Appl Phys 61:3577

2. Manaf A, Buckley RA, Davies HA, Leonowicz M (1991) J Magn Magn Mater 101:360
3. Kneller EF, Hawig R (1991) IEEE Trans Magn 27:3588
4. Skomski R (2003) J Phys Condens Matter 15:R841
5. Bertotti G (1998) Hysteresis in magnetism. Academic, San Diego
6. Branagan DJ, Kramer MJ, McCallum RW (1996) J Alloys Compd 244:27
7. Branagan DJ, McCallum RW (1996) J Alloys Compd 244:40
8. Branagan DJ, McCallum RW (1995) J Alloys Compd 230:67
9. Kramer MJ, Li CP, Dennis KW, McCallum RW, Sellers CH, Branagan DJ, Lewis LH, Wang JY (1998) J Appl Phys 83: 6631
10. Chang HW, Chiu CH, Chang WC (2003) Appl Phys Lett 82:4513
11. Hirosawa S, Kanekiyo H, Uehara M (1993) J Appl Phys 73:6488
12. Uehara M, Konno TJ, Kanekiyo H, Hirosawa S, Sumiyama K, Suzuki K (1998) J Magn Magn Mater 177–181:997
13. Hinomura T, Nasu S, Kanekiyo H, Uehara M, Hirosawa S (1997) J Jpn Inst Met 61:765
14. Barra-Barrera AD, Murakami RK, Villas-Boas V (2001) J Magn Magn Mater 226–230:1428
15. Barra-Barrera AD, Murakami RK, Partiti CSM, Villas-Boas V (2001) J Magn Magn Mater 226–230:1426
16. Ishii R, Miyoshi T, Kanekiyo H, Hirosawa S (2006) IEEE Int Magn Conf Dig 912. doi:10.1109/INTMAG.2006.374943
17. de Franco VC, Murakami RK, Rechenberg HR, Yonamine T, Missell FP, Villas-Boas V (2008) IEEE Trans Magn 44:4258
18. Cornejo DR, Peixoto TRF, Reboh S, Fichtner PFP, de Franco VC, Villas-Boas V, Missell FP (2010) J Magn Magn Mater 322:827
19. Murakami RK, Rechenberg HR, Neiva AC, Missell FP, Villas-Boas V (2008) J Magn Magn Mater 320:e65
20. Murakami RK, Rechenberg HR, Villas-Boas V, McCallum RW (2006) J Appl Phys 99:08B501
21. Skomski R, Coey JMD (1993) Phys Rev B 48:15812
22. Heslop D, Muxworthy AR (2005) J Magn Magn Mater 288:155
23. Pike CR (2003) Phys Rev B 68:104424
24. Pike CR, Ross CA, Scalettar RT, Zimanyi G (2005) Phys Rev B 71:134407
25. Cornejo DR, Noce RD, Peixoto TRF, Barelli N, Sumodjo PTA, Benedetti AV (2009) J Alloys Compd 479:43
26. Hirosawa S, Kanekiyo H, Miyoshi T (2004) J Magn Magn Mater 281:58
27. Skomski R, Coey JMD (1993) IEEE Trans Magn 29:2860
28. Andrei P, Caltun O, Stancu A (2006) Physica B 372:265
29. Chiriac H, Lupu N, Stoleriu L, Postolache P, Stancu A (2007) J Magn Magn Mater 316:177
30. Davies JE, Hellwig O, Fullerton EE, Jiang JS, Bader SD, Zimányi GT, Liu Kai (2005) Appl Phys Lett 86:262503
31. Stancu A, Stoleriu L, Cerchez M (2001) J Appl Phys 89:7260